ELSEVIER

Contents lists available at ScienceDirect

# Materials & Design

journal homepage: www.elsevier.com/locate/matdes



# A general phase-field framework for predicting the structures and micromechanical properties of crystalline defects



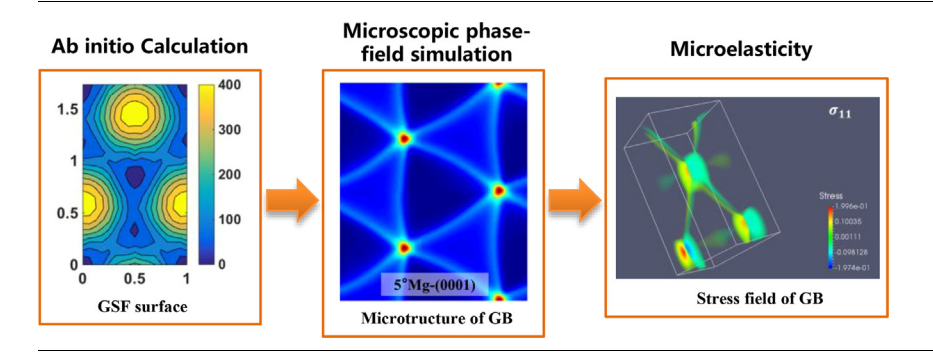
Di Qiu<sup>a</sup>, Pengyang Zhao<sup>b,\*</sup>, Yunzhi Wang<sup>c</sup>

- <sup>a</sup> Materials Genome Institute, Shanghai University, 333 Nan Chen Road, Shanghai 200444, China
- <sup>b</sup> Department of Engineering Mechanics, School of Naval Architecture, Ocean & Civil Engineering, Shanghai Jiao Tong University, 800 Dongchuan Road, Shanghai 200240, China
- <sup>c</sup>Department of Materials Science and Engineering, The Ohio State University, 2041 College Road, Columbus, OH 43210, USA

#### HIGHLIGHTS

- A phase-field framework is provided to bridge defect structures to properties.
- Model input can be solely determined by atomistic calculations.
- The predicted stress field of defects can be directly used in mesoscopic analysis.

#### G R A P H I C A L A B S T R A C T



### ARTICLE INFO

Article history: Received 27 May 2021 Revised 28 June 2021 Accepted 4 July 2021 Available online 7 July 2021

Keywords: Microstructure Dislocation Grain boundary Stress field Magnesium

# ABSTRACT

This work provides a phase-field simulation framework that bridges the structure of defects (e.g., dislocations and grain boundaries (GBs)) to their characteristic properties, such as stresses and energies. The validity of the current methodology is examined first by predicting the stress field of a single infinitely long screw dislocation using both the analytical solutions based on anisotropic elasticity and the current phase-field framework. The well-known stress singularity associated with the dislocation core in the former method has been effectively avoided in the latter. The framework is then applied to predicting the dislocation network of {0 0 0 1} twisted GB in Mg, which is found to consist of triangular-shaped regions of stacking faults and perfect crystals separated by partial dislocations. This prediction is consistent with some existing atomistic simulations and the underlying formation mechanism is analyzed rigorously using the displacement field predicted by our model, revealing the energy minimization process via the dissociation of a  $\begin{pmatrix} 1 & 1 & 2 & 0 \end{pmatrix}/3$  screw dislocation into a pair of  $\langle 1100 \rangle/3$  screw dislocations. Based on the structure prediction, the associated stress field is further simulated, which provides critical information in evaluating the interaction of GBs and other crystalline defects such as impurities and dislocations.

© 2021 The Authors. Published by Elsevier Ltd. This is an open access article under the CC BY-NC-ND license (http://creativecommons.org/licenses/by-nc-nd/4.0/).

#### 1. Introduction

The exhibiting properties of polycrystalline crystals depend crucially on the grain boundaries (GBs), which poses a great challenge

\* Corresponding author.

E-mail address: zhao.py@sjtu.edu.cn (P. Zhao).

for experiments to study *in situ* the subsequent microstructural evolution in response to external stimuli [1,2]. For example, a strong basal texture where the *c*-axis of Mg (HCP) grains aligned parallel to each other will lead to significant anisotropy in plastic deformation [3]. Special boundaries, such as low-angle GBs and low-CSL (Coincidence Site Lattice) boundaries, are found to have low vulnerability to cracking [4]. It has also been reported that

D. Qiu, P. Zhao and Y. Wang

Materials & Design 209 (2021) 109959

effective strengthening could be achieved without compromising ductility, electrical, or thermal properties by introducing coherent, stable, and nanoscale internal boundaries [5].

GBs exhibit many special properties that deviate from those of the bulk. For example, Simple twin boundaries in ferroelastic materials can be superconducting and multiferroic and exhibit other exclusive properties [6]. Strengthening polycrystalline materials has been effectively achieved through identifying structural characteristics for boundaries [7], since the structure of a GB determines all its essential properties, such as the diffusivity, mobility, cohesive strength, energy, local stress field, and their interactions with other stress-bearing extended defects such as dislocations, cracks, micro voids, and coherent precipitates [8]. On the other hand, crystalline defects, such as dislocations, grain boundaries, and slip lines tend to promote precipitation and allow for the creation of nano precipitate networks that offer unprecedented properties [9–12]. The key to predict such a guided precipitation is to accurately calculate the structure and the resulting elastic fields of these defects. Therefore, for many decades under the concept of grain boundary engineering [13,14], a lot of work has been done in predicting GB structures, including crystallographic theory, atomistic simulations, and ab initio calculations.

The conventional five degrees of freedoms (DOFs) of GBs, arising from misorientation of the two adjoining grains and the GB plane inclination, have been found insufficient to explain the properties and roles of GBs during processes such as phase transformations and plastic deformation. Instead, additional "internal" DOFs may need to be introduced to better describe GBs and understand the resulting effect [13-15]. The classical Frank-Bilby equation provides the net dislocation Burgers vector required to maintain the interface compatibility when crossing a GB [2,16,17]. The Olattice theory further quantizes this net Burger vector into lattice vectors of the reference crystal by taking into account the translational symmetry of the adjoining grains [18]. As a matter of fact, the Burgers vectors of GB dislocations are not necessarily to be integral multiple of lattice vectors. When the Coincidence Site Lattice (CSL) sites are considered, the Burgers vector can be fractional of lattice vectors, which is determined through the DSC lattice [19]. These theories are based purely on geometrical consideration and their applications to predicting real GB structures rely on some prior assumptions, such as the requirement of minimizing the dislocation content. On the other hand, molecular dynamics (MD) can be used to predict atomic structures and energies of GBs [20]. However, MD results essentially describe GB structures in terms of displacements of all atoms at and near the boundary, which are virtually impossible to be incorporated directly in any coarsegrained theories and models aiming to studying macroscopic properties controlled by GBs.

Following the spirit of multi-scale modeling in computational materials science, it is highly desired that a model can combine the existing geometric models (e.g., Frank-Bilby equation and Olattice) with the atomistic energetics provided by first-principle calculations to predict both GB structure and properties such as the energy and stress field, which can then be easily incorporated into mesoscale models such as phase-field (to study the GB effect on microstructure evolution [12]) and crystal plasticity (to study the GB effect on plastic deformation [21,22]). The need and significance of such development is only becoming apparent in recent years and more theoretical and modeling effort is expected. Recently, a novel microscopic phase-field (MPF) method with subatomic resolution is developed and applied to calculating the dislocation network in pure Al [23], evaluating the transition in GB structures in various BCC metals [24], and investigating dislocation structures [33] and dynamics [34]. Nevertheless, application of this new model to grain boundaries in HCP metals has not been carried out. Besides, previous applications have not studied the resulting stress field associated with the defects. In this paper, we will address these two issues within the context of considering the formation of dislocation network in twist GBs in Mg (owing to its significance to developing lightweight metal components in recent years). A brief description of the model framework, together with the model setups and inputs used in the current simulations, is given in Section 2. In Section 3, the stress field of the nonsingular infinitely long straight dislocation is calculated and compared with the analytical solution as a benchmark, following which the model is applied to studying the formation and stress field of the dislocation network at the twist GBs in Mg. These results and corresponding discussion are presented in Section 3, with major conclusions summarized in Section 4.

#### 2. Methods

### 2.1. Structure prediction using a microscopic phase-field model

The microscopic phase-field (MPF) theory [23] was recently developed to account for a continuum description of crystalline defects such as dislocations and GBs at the atomistic scale so that characteristics of those defects (e.g., dislocation core structure, grain boundary energy, etc.) will be the output of MPF, rather than the input as in the conventional mesoscale models. This is achieved by removing the gradient term and replacing the bulk free energy in the traditional phase-field model with a crystalline energy  $E^{\rm cryst}$  that is based on atomistic calculations. Therefore, the total free energy in MPF model can be written as:

$$E^{\text{tot}} = E^{\text{cryst}} + E^{\text{el}} + W \tag{1}$$

Similar to the principal idea of Peierls model for dislocations [25], while the  $E^{\text{cryst}}$  in the MPF model is constrained within the GB plane (GBP), the  $E^{\text{el}}$  is stored in the entire crystal. The equilibrium defect structure is then given as a result of the balance between  $E^{\text{cryst}}$  (localized) and  $E^{\text{el}}$  (nonlocal). In particular, the former is associated with the nonlinear and nonconvex generalized stacking fault (GSF):

$$E^{\text{cryst}} = \int \gamma[\mathbf{u}(x, y)] dxdy \tag{2}$$

where  $\gamma[\mathbf{u}(x,y)]$  is the GSF energy that depends on the inelastic displacement vector  $\mathbf{u}(x,y)$ . Following the spirit of Peierls model for dislocations [25], we assume that  $\mathbf{u}(x,y)$  is a planar quantity confined in the fault plane and serves as the displacement basis vector, which can be expressed as:

$$\mathbf{u}(x,y) = \sum_{p=1}^{N} \mathbf{b}^{p} \phi_{p}(x,y)$$
 (3)

a summation over all active slip systems, each characterized by a planar order parameter field  $\phi_p(x,y)$ . Here  $\mathbf{b}^p$  is a basis (eigen) displacement vector within the p-th slip system and N is the number of total active slip systems. This equation is analogous to the conventional phase-field dislocation theory where the inelastic transformation strain field is given as

$$\varepsilon_{ij}^{\mathrm{T}}(\mathbf{r}) = \sum_{p=1}^{N} \varepsilon_{ij}^{p} \eta_{p}(\mathbf{r})$$
 (4)

Here  $\varepsilon_{ij}^p = \left(n_i^p b_j^p + n_j^p b_i^p\right)/(2d^p)$  is the (constant) strain tensor associated with the p-th slip system.  $n^p$  and  $d^p$  are respectively the normal and interplanar spacing of slip planes, and  $\eta_p(\mathbf{r})$  is a phase field that resides within the 3D volume in general. When  $\eta(\mathbf{r}) = \phi_p(x,y)\delta(z-z_s)d^p$ , i.e., only distributed in the slip plane,

 $\varepsilon_{ij}^{\mathrm{T}}(\mathbf{r})$  is reduced to the inelastic displacement vector  $\mathbf{u}(x,y)$ . On the other hand, the elastic energy stored in the 3D volume of crystal is given in general as

$$E^{\text{el}} = E^{\text{el}} \Big[ \eta_p(\mathbf{r}) \Big] = \frac{1}{2} \sum_{p,q=1}^{N} \int B_{pq} \Big( \hat{\mathbf{g}} \Big) \widetilde{\eta}_p(\mathbf{g}) \widetilde{\eta}_q^*(\mathbf{g}) \frac{d\mathbf{g}}{(2\pi)^3}$$
 (5)

where  $\mathbf{g}$  is the reciprocal vector,  $\widehat{\mathbf{g}} \equiv \mathbf{g}/|\mathbf{g}|$ , and  $B_{pq}(\widehat{\mathbf{g}}) = C_{ijkl}\epsilon_{ij}^p\epsilon_{kl}^q - n_i\sigma_{ij}^p\Omega_{jk}(\widehat{\mathbf{g}})\sigma_{kl}^qn_l$ . The tilde  $\sim$  designates the Fourier transform and the asterisk a complex conjugate,  $\sigma_{ij}^p \equiv C_{ijkl}\epsilon_{kl}^T$  with  $C_{ijkl}$  being the elastic stiffness tensor, and  $[\Omega_{ik}]^{-1}(\widehat{\mathbf{g}}) \equiv C_{ijkl}\widehat{g}_j\widehat{g}_l$ . Note that additional condition  $\eta(\mathbf{r}) = \phi_p(x,y)\delta(z-z_s)d^p$  should be applied to Eq. (5) in order to obtain the final closed-form solution of  $E^{\text{el}}$  (see [23] for more details). Since both  $E^{\text{el}}$  and  $E^{\text{cryst}}$  are functionals of  $\phi_p(x,y)$ , the relaxation of the GB structure can be described using the Allen-Cahn equations, which reaches the equilibrium state when the variation of the total energy becomes zero.

## 2.2. Stress calculation using the phase-field microelasticity theory

In order to calculate the stress state of an elastic medium containing dislocations of arbitrary shapes and distributions, the key problem is to solving the stress equilibrium equation, i.e.,

$$\sigma_{ii,i}(\mathbf{r}) = 0 \tag{6}$$

subjected to the prescribed boundary conditions. Here we briefly describe the computation procedure. First, define the displacement field and the total strain field as  $u_i(\mathbf{r})$  and  $\epsilon_{ij}(\mathbf{r})$ , which according to the elasticity theory (under infinitesimal strain assumption), are related by

$$\epsilon_{ij}(\mathbf{r}) = \frac{1}{2} \left[ u_{i,j}(\mathbf{r}) + u_{j,i}(\mathbf{r}) \right] \tag{7}$$

The elastic strain is part of the total strain and expressed as

$$e_{ij}(\mathbf{r}) = \epsilon_{ij}(\mathbf{r}) - \varepsilon_{ij}^{\mathrm{T}}(\mathbf{r})$$
 (8)

where  $\varepsilon_{ij}^{\mathrm{T}}(\mathbf{r})$  is the inelastic strain field determined by the strain tensor and the distribution of dislocations in the specified slip systems, as shown in Eq. (4). By substituting Eqs. (7) and (8) into the the stress equilibrium equation (Eq. (6)) and using the constitutive relationship  $\sigma_{ij}(\mathbf{r}) = C_{ijkl}e_{kl}(\mathbf{r})$  together with the symmetry of the elastic stiffness tensor  $C_{ijkl}$ , we have

$$\left(C_{ijkl}u_{k,l}(\mathbf{r}) - \varepsilon_{kl}^{T}(\mathbf{r})\right)_{i} = 0 \tag{9}$$

Solving Eq. (9) gives the displacement, stress, and strain fields of the given dislocation configuration. In order to solve this set of second order partial differential equations, the spectral method based on fast Fourier transform is employed, which can greatly improve the computational efficiency. Note that Eq. (9) is a general form regardless of the location dependence of  $C_{ijkl}$ . For elastically homogeneous system (e.g., an infinite crystal containing a single dislocation), a closed-form solution has be derived in [26] and the corresponding numerical implementation is straightforward. For a bi-crystal containing a GB (to be considered in the current study), the elastic stiffness tensors of the two grains are different and related according to the crystallographic orientation of the GB. For such an elastically inhomogeneous system, no closed-form solution exists for Eq. (9) and the method proposed in Ref. [27] is implemented numerically to obtain the stress equilibrium fields. Note that the inelastic field  $\varepsilon_{ii}^{T}(\mathbf{r})$  in Eq. (8) is the input of the model, which contains the characteristic information of defects in calculating the stress field and in the current work is uniquely predicted using MPF simulations.

#### 2.3. Model setup and inputs

To calculate the GB dislocation network in a pure twist GB in Mg, we will first validate the MPF method by modeling the structure of a single dislocation and then calculating its stress field and comparing with the analytical solution. Note that the analytical solution of dislocation stress field is based on the assumption of a singular non-dissociated core, which is contrary to the dissociated core structure of basal dislocations in Mg (as will be discussed latter in this paper). For the benchmark purpose, we perform the MPF and stress field simulations instead for the single dislocation in {111} plane of Al crystal, which, due to a relatively high sacking fault energy, results in virtually no dissociation in the dislocation cores. Note that both {0 0 0 1} of Mg and {111} of Al are close-packed planes sharing certain crystallographic similarity.

As two types of crystal defects will be investigated in the present work, i.e., the core structure of single screw dislocation in Al and the dislocation network of a pure twist GB in the basal plane of Mg, their corresponding model parameters are listed in Table 1. Another important model input, the GSF surfaces of  $\{111\}_{Al}$  and  $\{0001\}_{Mg}$  (will be shown in the subsequent section), can be found in Refs. [23] and [29], respectively.

The simulation cells of the single screw dislocation and the basal twist GB are shown in Fig. 1(a) and (b), respectively. The screw dislocation is located on the closed packed plane  $(1 \ 1 \ 1)_{Al}$ with its Burgers vector in the direction of  $\begin{bmatrix} 0 & 1 & \bar{1} \end{bmatrix}_{Al}$ . Assuming that the displacement along the dislocation sense direction is identical, the three-dimensional simulation cell could be reduced to a twodimensional one (indicated by the dashed square in Fig. 1(a)). The twist GB at the basal plane of Mg crystal is considered as generated due to a rotation of Grain-A by 5° relative to the Grain-B around their common  $[0\ 0\ 0\ 1]_{Mg}$  direction. The system size in terms of  $l_1$ ,  $l_2$ , and  $l_3$ , together with the grid size  $l_0$  is shown in Table. 1. Note that considering the symmetry of the HCP crystal, the model unit cell (i.e., the green square in Fig. 1(b)) is selected from the GBP in order to comply with the periodic boundary condition required for the MPF model when Fourier transformation is applied to calculating the elastic energy in Eq. (5).

As an input of MPF model, discrete GSF data (Fig. 1(c)) of Mg basal plane from *ab initio* calculations [29] is firstly fitted using a truncated Fourier series and shown in Fig. 1(d) in order to be used in the simulation grid with a much finer resolution. The minima are located at the centers of the triangular contours and correspond to the lattice sites of the (0 0 0 1) plane in Mg. It should be noted that the plots in Fig. 1(c) and (d) have the smallest unit cell with the periodicity being [1 1  $\bar{2}$  0]/3 and  $\bar{1}$  1 0 0 along two orthogonal crystal directions; when the GSF data is applied to the MPF model, it needs to be extended according to the simulation cell (i.e., GB plane indicated in Fig. 1(b)).

#### 3. Results and discussion

# 3.1. Model validation: Calculating the stress field of a single screw dislocation

Based on the fundamental of phase-field method, the screw dislocation with the initial configuration is shown in Fig. 1(a). The left and right halves divided by the dislocation line represent the slipped and non-slipped regions, wherein the order parameters are set as  $\phi=1$  and  $\phi=0$  (unit: b), respectively. When the system starts to evolve under the interplay of the crystalline energy and elastic strain energy, the sharp dividing interface containing the initial dislocation line gradually becomes a diffused region with a certain width. Assuming that the elastic state along the dislocation

**Table 1**Model parameters for the single screw dislocation in Al and the twist GB network in Mg.

Model parameters	Single screw dislocation in {111} <sub>Al</sub>		Twist GB network in {0 0 0 1} <sub>Mg</sub>		Unit
Lattice parameter	$a_0$	0.405	$a_0, c_0$	0.321, 0.521	nm
Grid size	$l_0$	0.0234	$l_0$	0.0261	nm
System size	$l_1, l_2, l_3$	$10240l_0$ , $1024l_0$ , $l_0$	$l_1, l_2, l_3$	$1024l_0$ , $244l_0$ , $140l_0$	nm
Elastic constants	$C_{11}, C_{12}, C_{44}$	108.2, 61.3, 28.5 [28]	$C_{11}$ , $C_{33}$ , $C_{44}$ , $C_{12}$ , $C_{13}$	60.0, 61.0, 18.1, 21.0, 20.0 [29]	GPa

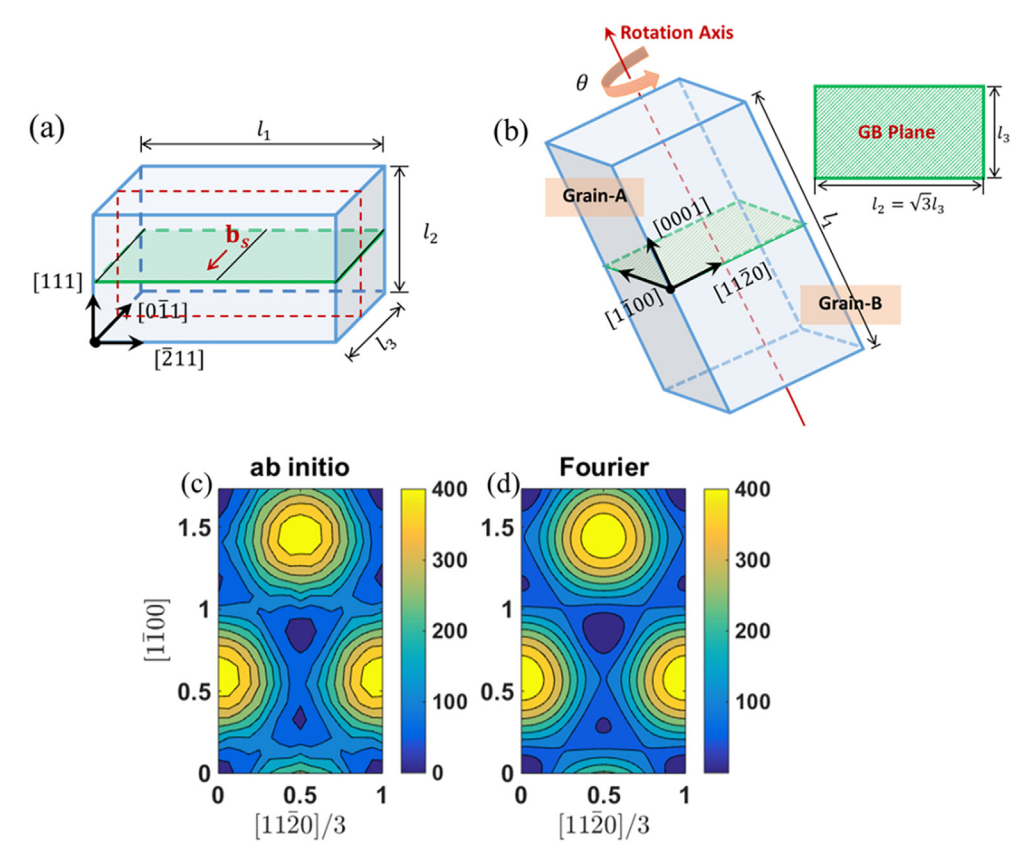


Fig. 1. The crystallographic characters of (a) single screw dislocation in Al and (b) pure twist (0 0 0 1)-GB in Mg; (c) and (d) are the original and fitted GSF profiles of Mg.

line is identical, the cross section of the 2-D dash square (in Fig. 1 (a)) perpendicular to the dislocation line is taken as our simulation cell. The profile of the disresgistry (i.e., the profile of order parameter  $\phi$ ) and the density of Burgers vector across the core center of the dislocation at the equilibrium are plotted in Fig. 2(a). When moving far away from the initial place of the dislocation (y=0), the density of Burgers vector decays to 0, indicating no distortion remains at the far-field.

Substituting order parameter profile into Eq. (4) gives the inelastic energy field  $\varepsilon_{ij}^T(\mathbf{r})$ . By solving the equilibrium equation (Eq. (9)) numerically, we obtain the stress field of the screw dislocation, of which the components,  $\sigma_{12}$  and  $\sigma_{13}$ , are shown in Fig. 2 (b) and (c). The analytical solution of the stress field for the screw dislocation (Fig. 1(a)) with a singular core has been derived based on anisotropic elasticity [28], the results of which are plotted in Fig. 2(b) and (c) (in red) to compare with our MPF calculation. Note that owing to the singularity, stresses from the analytical solution clearly show divergence in the core region, as indicated in Fig. 2(b) and (c). Comparing the numerical calculation based on the MPF with the analytical solutions, it is obvious that the former exhibits a smooth and finite variation across the core region with the absence of stress singularity. Outside the core, the stresses decay quickly to zero as moving towards the far field in both cases; the

numerical results of the MPF method fit well with those by the analytical solutions in regions with a distance  $\geq 2.5b$  from the core center. This is consistent with the assumption that the elasticity theory is only validate out of the core region with a radius of  $\sim 2b$  [28]. Therefore, the current MPF description provides an accurate description of dislocation structures, which allows us to further apply it to predicting more complex configurations of dislocation networks. In addition, since the microstructures are described using order parameters, by employing the numerical method presented in Section 2.2, one can obtain the stress field of dislocations or other defects of arbitrary configurations, which is difficult to calculate using the linear elasticity method as the corresponding analytical solution is only available when the geometry of the dislocation configuration satisfies certain symmetry requirements [28].

# 3.2. Dislocation network structure of pure twist (0001) grain boundary in Mg

Consider a pure-screw twist GB parallel to the basal plane with a misorientation angle  $\theta$  ( $\theta=5^{\circ}$  in this work), whose construction has been outlined in Section 2.3 and illustrated in Fig. 1(b). This results in a relative displacement

D. Qiu, P. Zhao and Y. Wang

Materials & Design 209 (2021) 109959

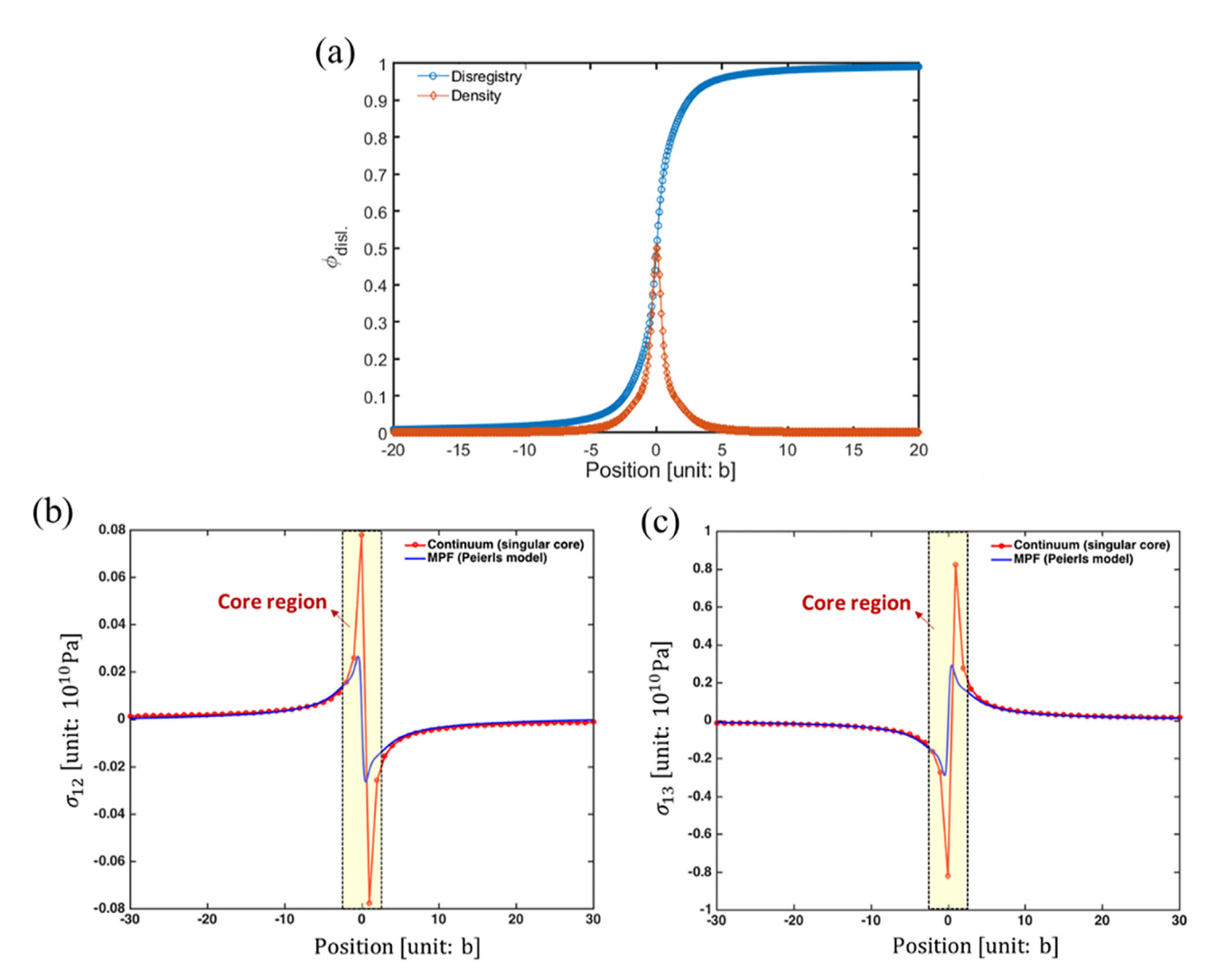


Fig. 2. The calculated configuration and stress fields of a single dislocation: (a) disregistry (in blue) and density of Burgers vector (in red), (b) and (c) the comparison between the stress field components from numerical calculations based on phase-field method (in blue) and from analytical solutions (in red) [28]. (For interpretation of the references to colour in this figure legend, the reader is referred to the web version of this article.)

$$\mathbf{u}_{\mathsf{R}}(x,y) = [\mathbf{R}(\theta) - \mathbf{I}](x,y) \tag{10}$$

where  $\mathbf{R}(\theta)$  is the rotation matrix and  $\mathbf{I}$  is the identity matrix. Such rigid-body rotation corresponds to the initial field of  $\mathbf{u}(x,y)$  in Eq. (2), which gives rise to the inelastic displacement field localized in the GBP but does not contribute to the elastic energy. In the MPF framework, the displacement  $\mathbf{u_R}$  can also be expressed in the form of Eq. (3). It has been proved in our previous work [24] that the choice of the basis displacement vectors in Eq. (3) can be arbitrary as long as they are all lying in the basal plane and non-collinear. The corresponding order parameter  $\phi(x,y)$ , known as the "background field" [23] and can be derived immediately by equating Eq. (3) and Eq. (10), provides the characteristic geometric constraint (i.e., the prescribed twist angle  $\theta$  in the current case) to regulate the energy minimization process in our MPF simulation.

In Fig. 3(a)–(e) we plot the distribution of crystalline energy that reflects the evolving structure of GB dislocations from the initial stage to the equilibrium. In these figures "O" represents the origin where the rotation axis passes through, i.e., the displacement at "O" is zero. At the early stage of t=2 (where t is the dimensionless time), the GB structure maintains the characteristics of the GSF profile, where the high energy regions, the transition regions (with relatively lower energy) and the non-slipped region ( $E^{cryst}=0$ ) are alternatingly arranged and a three-fold symmetry can be easily

identified. As the evolution advances, the high energy regions gradually shrink and is connected by the transition regions, which expand to form triangular areas. At the equilibrium state (t = 100), it can be found that instead of sharp and well-defined dislocation lines, the dislocations locate near the edges of the triangular areas and spread into the center of these triangular regions of faulted material. The crystalline energy (see Fig. 3(f)) decreases monotonically to a plateau but contributes the most to the GB energy throughout the microstructural evolution, whereas the elastic energy is initially zero and gradually increases to a steady value. The interplay between the crystalline and elastic energy leads to a monotonic decrease of the GB energy until the equilibrium is reached.

#### 3.3. Geometric characteristics of GB dislocations

To identify the Burgers vectors of the "diffused" dislocations, the displacement field is calculated according to Eq. (3) at t=100. The direction and magnitude of the displacement at each field point is reflected by the white arrows in Fig. 4(a) with the equilibrium dislocation structure of GB (Fig. 3(e)) shown as the background. In general, the magnitude of displacement within the unit cell is proportional to the distance between the field point

D. Qiu, P. Zhao and Y. Wang

Materials & Design 209 (2021) 109959

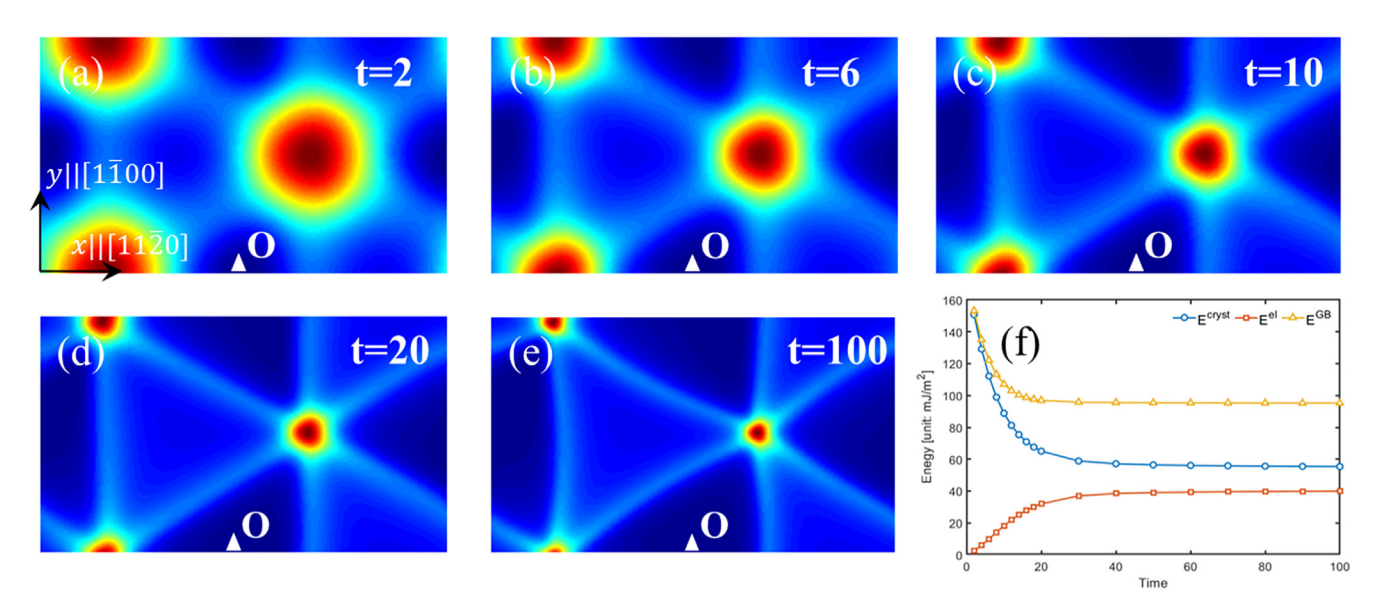


**Fig. 3.** Temporal evolution of crystalline energy (reflecting the temporal structure of GB dislocations) from t = 1 to t = 100 and the variations of energies (GB energy  $E^{GB}$ , elastic energy  $E^{el}$  and crystalline energy  $E^{eryst}$ ) during this evolving process.

and the origin. If we plot the displacement along OA and AB vectors (corresponding to 1 2 1 0 and 1 1 2 0, respectively), it can be found that across the dislocation L1, the displacement  $\mathbf{u}_{OA} = [-0.50, -0.28]a_0$ , and across dislocation L2, the displacement  $\mathbf{u}_{AB} = [0, -0.58]a_0$ , as shown in Fig. 4(b). This calculation indicates that the Burgers vectors associated with L1 and L2 are  $\mathbf{b}_1 = \begin{bmatrix} 1 & 0 & 1 & 0 \end{bmatrix}/3$  and  $\mathbf{b}_2 = \begin{bmatrix} 1 & 1 & 0 & 0 \end{bmatrix}/3$ , respectively, which are actually parallel to the dislocation lines of L1 and L2. Therefore, both dislocations exhibit the character of pure screw. Similarly, the Burgers vector of dislocation L3 can also be determined by calculating the difference of the displacements between the centers of adjacent triangular regions, which leads to  $\mathbf{b}_1 = \begin{vmatrix} 0 & 1 & 1 & 0 \end{vmatrix}/3$  and thus confirms its screw character. Therefore, it is clear that for Mg the dislocation network for pure twist (0 0 0 1)-GB is consisting of pure screw dislocations with line direction and Burgers vectors parallel to  $\langle 1 \ 1 \ 0 \ 0 \rangle$  directions.

The areas surrounded by these dislocations (i.e., L1, L2 and L3) are either the stacking fault (SF) or the perfect HCP structure (non-slipped region), as has been schematically shown in Fig. 5 (a). Our calculation results are consistent with a previous atomistic simulation [3]. On the other hand, the displacement between B and O is also identified,  $\mathbf{u}_{OB} = [-0.50, -0.86]a_0$ , corresponding to  $1/3\left\langle 1 \ 1 \ \bar{2} \ 0\right\rangle$ , which is also commonly observed Burgers vector for twist (0 0 0 1)-GB. For example, Tochigi et al. [30] observed pure screw dislocation network in the basal plane of  $\alpha$ -Al<sub>2</sub>O<sub>3</sub>with

Burgers vectors being  $1/3\langle 1\ 1\ \bar{2}\ 0\rangle$ . Fig. 5(b) shows the morphology of such dislocation network, with line direction indicated by blue lines and Burgers vectors by black arrows. From the perspective of crystallography and similar to the idea of "O-lattice" theory, non-slipped regions (indicated by O, O<sub>1</sub>, O<sub>2</sub> and O<sub>3</sub>) are separated by dislocations located in the middle of adjacent O regions, e.g., O-O<sub>1</sub>, O-O<sub>2</sub> and O-O<sub>3</sub>. However, in the current study, the  $1/3\langle 1\ 1\ \bar{2}\ 0\rangle$  ( $\mathbf{b}_i$  in Fig. 5(b)) is not observed, which instead is dissociated into two partial dislocations ( $\mathbf{b}_i^p$ ) due to the low stacking fault energy (34 mJ/m² according to the GSF data used in the current work [29]), i.e.,

$$1/3\left\langle 1 \ 1 \ \overline{2} \ 0\right\rangle \rightarrow 1/3\left\langle 0 \ 1 \ \overline{1} \ 0\right\rangle + 1/3\left\langle 1 \ 0 \ \overline{1} \ 0\right\rangle \tag{6}$$

The orientation and magnitude of the corresponding Burgers vectors are shown in Fig. 5(c). Such dissociation allows for the decomposition of screw dislocations along  $\langle 1\ 1\ \bar{2}\ 0\rangle$  (indicated by blue lines in Fig. 5(b)) and the formation of SF at the triple junctions (indicated by yellow triangles in Fig. 5(b)).

# 3.4. Stress field of the GB dislocation network

The GB dislocations, whose structures have been calculated and shown in Fig. 3(e), give rise to the GB energy as well as a longrange stress field, which will affect the diffusion, precipitation

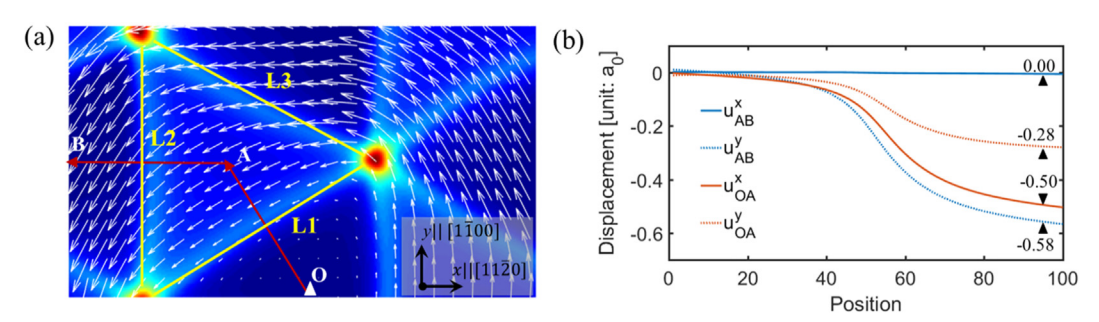


Fig. 4. (a) Displacement field and (b) variation of displacement components along dislocation segments L1 and L2.

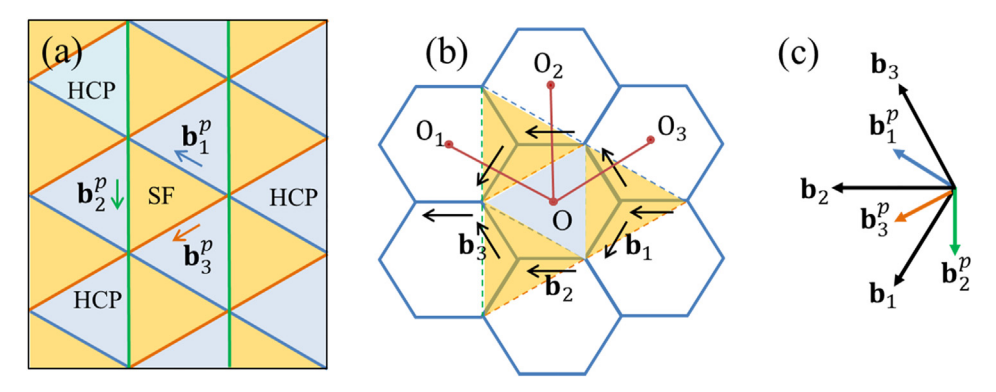


Fig. 5. Dissociation of basal dislocations: (a) three partial dislocations predicted by the current model, (b) illustration of the transformation in the basal dislocation networks from the honeycomb structure into a triangular structure, (c) schematics of the dislocation reaction of every two "end to end" basal dislocations with  $\mathbf{b}_i \parallel \left\langle 1 \ 1 \ \bar{2} \ 0 \right\rangle$  into partial ones with  $\mathbf{b}_i^p \parallel \left\langle 0 \ 1 \ \bar{1} \ 0 \right\rangle$ .

[10,11], and other processes associated with GBs. We use the method discussed in Section 2.2 to calculate the resulting 3D stress field based on the GB structure (Section 3.2) predicted by MPF, which is similar to the calculation in Section 3.1 for a single screw dislocation. The distributions of dislocation stress components are shown in Fig. 6. By comparing the stress distribution in Fig. 6 with the equilibrium configuration of dislocation work in Fig. 3(e), we find that the stress concentration occurs along the dislocation segments or at the nodal points of the dislocation network for all stress components. As has been studied in our previous work [11,12], such stress field provides an extra driving force for the subsequent nucleation of new phases and alters the microtexture near dislocations and GBs. As for Mg alloys, the effect of stress fields associated with basal dislocation networks on the formation of novel structures of precipitates has also been investigated [10]. However, instead of superposing the stress fields of small and straight dislocation segments using the linear elasticity theory under the assumption of elastically isotropic medium, our calculation gives a more accurate description of the stress field, especially that at the nodal point. In particular, the current method relies on the GB dislocation networks predicted by MPF and thus contains the possible nodal reactions and predicts a finite and smooth stress

variation across the dislocation cores. These features can be significant in the subsequent investigation of interaction between GBs and other defects, which is believed to play a dominant role in techniques based on grain boundary engineering [31,32]. In fact, our analysis in Section 3.3 on the possible dislocation dissociation reactions involved in the formation of GBs may imply a possible route for manipulating Mg-alloy properties via grain boundary engineering. Since the GSF energy is sensitive to the composition of materials, we may also be able to control the GB structure and hence the resulting stress field of Mg alloys by the addition of alloying elements with different types and amount, which may in turn affect the precipitation and segregation processes near GBs. For example, our previous work has shown that during dislocation/GB guided precipitation process in Ti- and Mg-alloys [10-12], the dislocation type, line direction, as well as the configuration of dislocation network will alter the nucleation sites and orientation of precipitates, thus leading to the formation of micro texture. Moreover, our most recent work also shows that the Gd atoms tend to segregate at the (0 0 0 1)-GBs in Mg-Gd alloy and form periodic pattern at/near the GB dislocation network, which will be shown in our future works.

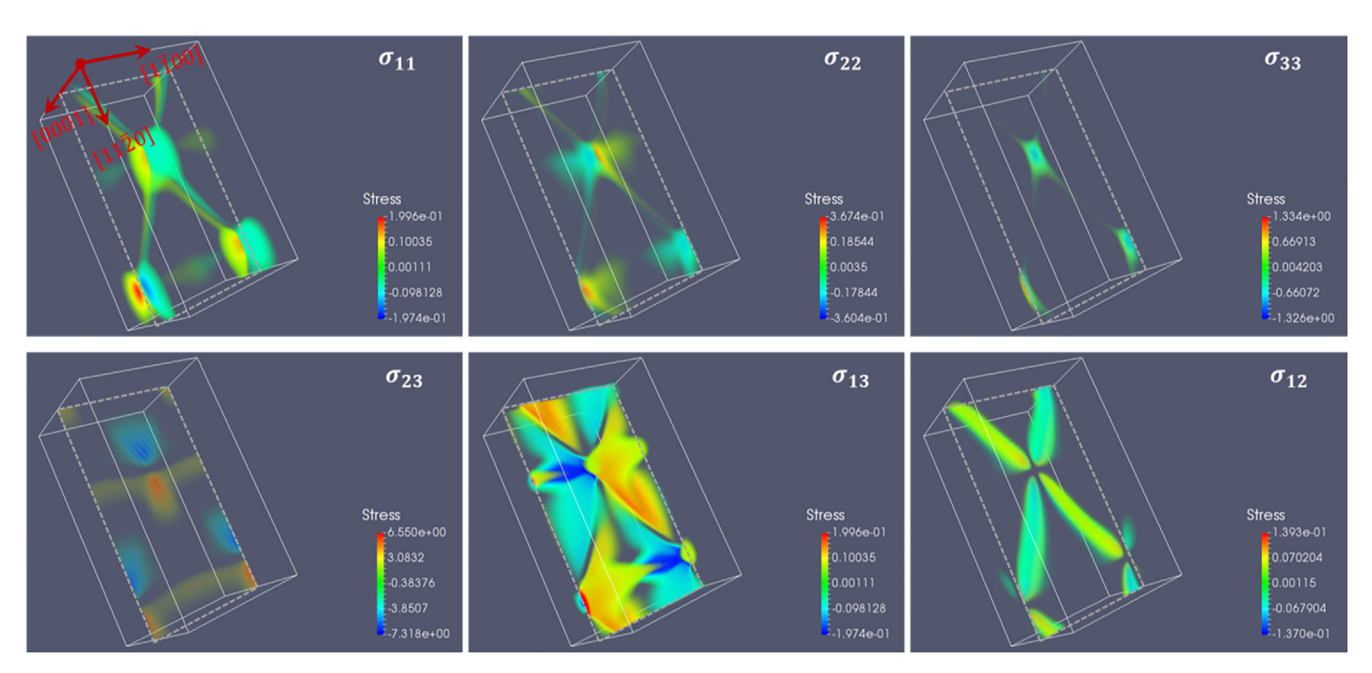


Fig. 6. Three-dimensional stress field of (0 0 0 1)-GB dislocation networks (in unit of GPa).

#### 4. Conclusions

By establishing a general phase-field framework, we are able to predict both the structures and micromechanical properties of common crystalline defects such as a single dislocation (demonstrated in aluminum) as well as dislocation networks of a grain boundary (demonstrated in magnesium). The main findings include:

- (1) The stress field of a single dislocation with a finite-sized core structure predicted by a microscopic phase-field model agrees well with that obtained from analytical solutions outside the core region (with a radius of  $\sim 2b$ , where b is the magnitude of Burgers vector), indicating a high precision achieved by the current phase-field methodology in predicting the structure of dislocations. Inside the core region, our method predicts finite stress values with smooth variation, suggesting its wider applicability than the classical analytical solution based on elasticity theory.
- (2) In addition, the Burgers vectors associated with dislocations are the output of the model rather than the input. Using the predicted displacement fields of dislocations, phase-field microelasticity can be directly used to calculate the stress field of dislocations with arbitrary configurations, removing the symmetry constraint imposed by the analytical solutions due to elastic anisotropy.
- (3) The twist (0 0 0 1)-GB in Mg consists of partial dislocations of pure screw character with Burgers vectors of  $\mathbf{b}_{i=1,2,3} = \langle 1 \ 1 \ 0 \ 0 \rangle / 3$ , among which stacking faults are formed. screw dislocations with  $\mathbf{b}_{i=1,2,3} = \langle 1 \ 1 \ 2 \ 0 \rangle / 3$  are found unable to form due to the high crystalline energy.

The current work presents a useful framework for calculating the stress field and energy of dislocations and GBs using the atomistic simulation data as the sole input, bridging the structural description of crystal defects to the micromechanics of the defects. The calculated stress field of these defects can be directly used in mesoscopic analysis and simulations for investigating grain boundary related phenomena such as grain boundary complexions and guided precipitation.

# **Declaration of Competing Interest**

The authors declare that they have no known competing financial interests or personal relationships that could have appeared to influence the work reported in this paper.

#### Acknowledgment

DQ would like to acknowledge the supports by the National Key Research and Development Program of China under grant number 2020YFB0704503 and the National Science Foundation of China under grant number 51801123; PZ would like to acknowledge the support by Shanghai Pujiang Program under grant number 20PJ1406500 (PZ); YW would like to acknowledge the support from U.S. National Science Foundation DMREF program under Grant number DMR 1922239.

#### References

[1] Y. Mishin, M. Asta, J. Li, Atomistic modeling of interfaces and their impact on microstructure and properties, Acta Mater. 58 (2010) 1117-1151.

- [2] A.P. Sutton, R.W. Balluffi, Interfaces in crystalline materials, 1995.
- X. Liu, J. Wang, Low-energy, mobile grain boundaries in magnesium, Sci. Rep. 6 (2016) 21393.
- Y. Pan, B.L. Adams, T. Olson, N. Panayotou, Grain-boundary structure effects on intergranular stress corrosion cracking of alloy X-750, Acta Mater. 44 (1996) 4685-4695.
- [5] L. Lu, Y. Shen, X. Chen, L. Qian, K. Lu, Ultrahigh strength and high electrical conductivity in copper, Science 304 (2004) 422-426.
- [6] X. Ding, Z. Zhao, T. Lookman, A. Saxena, E.K. Salje, High junction and twin boundary densities in driven dynamical systems, Adv. Mater. 24 (2012) 5385-
- [7] K. Lu, L. Lu, S. Suresh, Strengthening materials by engineering coherent internal boundaries at the nanoscale, Science 324 (2009) 349-352.
- [8] P.R. Cantwell, M. Tang, S.J. Dillon, J. Luo, G.S. Rohrer, M.P. Harmer, Grain boundary complexions, Acta Mater. 62 (2014) 1-48.
- [9] S.H. Kim, H. Kim, N.J. Kim, Brittle intermetallic compound makes ultrastrong low-density steel with large ductility, Nature 518 (2015) 77–79.
- [10] H. Liu, Y. Gao, Z. Xu, Y.M. Zhu, Y. Wang, J.F. Nie, Guided self-assembly of nanoprecipitates into mesocrystals, Sci. Rep. 5 (2015) 16530.
- D. Qiu, R. Shi, D. Zhang, W. Lu, Y. Wang, Variant selection by dislocations during  $\alpha$  precipitation in  $\alpha/\beta$  titanium alloys, Acta Mater. 88 (2015) 218–231.
- [12] D. Qiu, R. Shi, P. Zhao, D. Zhang, W. Lu, Y. Wang, Effect of low-angle grain boundaries on morphology and variant selection of grain boundary allotriomorphs and Widmanstätten side-plates, Acta Mater. 112 (2016) 347
- [13] Y. Ishida, M.H. Brown, Dislocations in grain boundaries and grain boundary sliding, Acta Metall. 15 (1967) 857-860.
- D. Raabe, M. Herbig, S. Sandlöbes, Y. Li, D. Tytko, M. Kuzmina, et al., Grain boundary segregation engineering in metallic alloys: a pathway to the design of interfaces, Curr. Opin. Solid State Mater. Sci. 18 (2014) 253-261.
- [15] L. Wang, J. Teng, P. Liu, A. Hirata, E. Ma, Z. Zhang, et al., Grain rotation mediated by grain boundary dislocations in nanocrystalline platinum, Nature Commun. (2014) 4402.
- [16] B.A. Bilby, R. Bullough, E. Smith, Continuous distributions of dislocations: a new application of the methods of non-Riemannian geometry, Proc. R. Soc. A: Math., Phys. Eng. Sci. 231 (1955) 263-273.
- [17] F.C. Frank, Martensite, Acta Metall. 1 (1953) 15-21.
- [18] W. Bollmann, Crystal Defects and Crystalline Interfaces, Springer Science & Business Media, 2012.
- A. Sutton, R. Balluffi, Overview no. 61 On geometric criteria for low interfacial energy, Acta Metall. 35 (1987) 2177-2201.
- [20] H. Van Swygenhoven, Grain boundaries and dislocations, Science 296 (2002) 66-67.
- [21] A. Ma, F. Roters, D. Raabe, On the consideration of interactions between dislocations and grain boundaries in crystal plasticity finite element modeling theory, experiments, and simulations, Acta Mater. 54 (2006) 2181-2194.
- [22] P. Zhao, T.S.E. Low, Y. Wang, S.R. Niezgoda, An integrated full-field model of concurrent plastic deformation and microstructure evolution: Application to 3D simulation of dynamic recrystallization in polycrystalline copper, Int. J. Plast. 80 (2016) 38-55.
- [23] C. Shen, J. Li, Y. Wang, Predicting structure and energy of dislocations and grain boundaries, Acta Mater. 74 (2014) 125–131.
- [24] D. Qiu, P. Zhao, C. Shen, W. Lu, D. Zhang, M. Mrovec, et al., Predicting grain boundary structure and energy in BCC metals by integrated atomistic and phase-field modeling, Acta Mater. 164 (2019) 799-809.
- R. Peierls. The size of a dislocation, Proc. Phys. Soc. 52 (1940) 34.
- [26] A.G. Khachaturyan, Theory of Structural Transformations in Solids, 1983.
- [27] Y.U. Wang, Y.M. Jin, A.G. Khachaturyan, Phase field microelasticity theory and modeling of elastically and structurally inhomogeneous solid, J. Appl. Phys. 92 (2002) 1351-1360.
- [28] J.P. Hirth, Theory of dislocations, J. Appl. Mech. 50 (1983) 476.
- [29] J.A. Yasi, L.G. Hector, D.R. Trinkle, First-principles data for solid-solution strengthening of magnesium; from geometry and chemistry to properties, Acta Mater. 58 (2010) 5704–5713.

  [30] E. Tochigi, Y. Kezuka, N. Shibata, A. Nakamura, Y. Ikuhara, Structure of screw
- dislocations in a (0001)/[0001] low-angle twist grain boundary of alumina ( $\alpha\text{--}$ Al2O3), Acta Mater. 60 (2012) 1293-1299.
- [31] M. de Koning, R.J. Kurtz, V.V. Bulatov, C.H. Henager, R.G. Hoagland, W. Cai, et al., Modeling of dislocation-grain boundary interactions in FCC metals, J. Nucl. Mater. 323 (2003) 281-289.
- [32] T. Watanabe, An approach to grain boundary design for strong and ductile
- polycrystals, Res Mech. 11 (1984) 47–84. [33] Di Qiu, Pengyang Zhao, Dallas Trinkle, Yunzhi Wang, Stress-dependent dislocation core structures leading to non-Schmid behavior, Materials Research Letters (2021)134-140, https://doi.org/10.1080/ 21663831.2020.1854359.
- [34] Pengyang Zhao, Chen Shen, Michael Savage, Ju Li, Stephen Niezgoda, Michael Mills, Yunzhi Wang, Slip transmission assisted by Shockley partials across  $\alpha/\beta$ interfaces in Ti-alloys, Acta Materialia 171 (2019) 291-305, https://doi.org/ 10.1016/j.actamat.2019.04.013.